Recursive function for fitting electroactive monolayer cyclic voltammograms and extracting key parameters

Olivier Alévêque, Eric Levillain

Recursive Function for Fitting Electroactive Monolayer Cyclic Voltammograms and Extracting Key Parameters

Olivier Alévêque and Eric Levillain

Univ Angers, CNRS, MOLTECH-ANJOU, SFR MATRIX, F-49000 Angers, France

Corresponding authors:

olivier.aleveque@univ-angers.fr (Olivier ALEVEQUE)

Tel.: (+33)241735090; Fax: (+33)241735405

eric.levillain@univ-angers.fr (Eric LEVILLAIN)

Tel.: (+33)241735095; Fax: (+33)241735405

ARTICLE INFO

Keywords:

Cyclic voltammetry

Curve fitting

Electroactive monolayers

Lateral interactions

Electrochemical simulations

ABSTRACT

This study introduces the rec-GLI function, a recursive function, aimed at accurately fitting cyclic voltammograms (CVs) under Nernstian conditions and estimating key parameters on electroactive monolayers or redox-responsive materials. The rec-GLI function is derived from the GLI model and improves upon previous functions by incorporating mathematical recursion and curve fitting algorithms implemented in Python and MATLAB.

A comparative analysis is conducted between the rec-GLI function and the GLI function, demonstrating the superior accuracy of the former in fitting CVs and estimating key parameters such as peak potential, peak intensity, full width at half maximum, surface coverage, and lateral interactions. The rec-GLI function proves particularly effective in cases where the peaks exhibit narrow widths and exhibits agreement with experimental data.

1. Introduction

Since their initial discovery in 1946 [1], Self-Assembled Monolayers (SAMs) have attracted considerable attention as fascinating systems for creating functionalized interfaces with diverse

applications in catalysis, energy storage, biosensing, and more. They have also become an ideal system for the theoretical study of interfacial phenomena, especially in the field of electrochemistry [2]. However, SAMs face challenges related to stability due to the nature of the binding between the molecules and the surface [3,4]. To address this issue, a popular and more recent method for constructing monolayers involves the use of diazonium salts [5]. These salts can form (self-assembled) monolayers of aryl groups through the reduction of the diazonium moiety [6,7].

Cyclic voltammetry (CV) is a powerful electrochemical technique widely used to study the redox behaviour of various systems, including monolayers composed of electroactive molecules exhibiting redox properties [8,9]. Accurate determination of CV parameters such as peak potentials, peak currents, and peak shapes is crucial for characterizing the redox and non-redox processes within monolayers, including the estimation of lateral interaction parameters that provide valuable insights into the molecular-level interactions, enhance our understanding of redox processes, and optimize monolayer-based devices [10–13].

Interpreting CV data for electroactive monolayers (EMs) requires robust fitting algorithms capable of extracting meaningful electrochemical parameters. However, fitting the CV peaks of these systems can be challenging due to the presence of lateral interactions between neighbouring molecules. These interactions strongly influence the electrochemical response, resulting in sharper or broader voltammetric peaks [14], and introduce mathematical complexities. In our previous works, we introduced novel mathematical functions to capture the effects of lateral interactions in the CV peaks of SAMs and EMs. One notable function is the Generalized Lateral Interactions (GLI) function [15], which successfully accounted for the complexities arising from intermolecular interactions and significantly simplified the fitting process compared to other existing models [16–18]. However, the GLI function employed certain approximations to simplify the mathematical recursions induced by the interactions, potentially reducing precision in some cases.

Building upon our previous findings, the present study aims to further refine the mathematical function for fitting CV peaks of EMs while preserving the mathematical recursion, for a redox reaction described by Butler-Volmer (BV) kinetic formalism under Nernstian conditions. This refinement will involve combining experimental CV measurements, advanced mathematical modelling techniques, and curve fitting algorithms implemented in Python and MATLAB. By doing so, we aim to unravel the complex interplay between lateral interactions and the electrochemical behaviour of EMs. The improved accuracy in parameter estimation will allow for a deeper understanding of the intricate intermolecular interactions within these systems, ultimately paving the way for the design and development of monolayer-based devices with enhanced electrochemical performance.

The following sections present an overview of the experimental conditions and theoretical background (section 2), details of the generalized lateral interaction (GLI) model and the recursive GLI function (rec-GLI) (sections 3 and 4, respectively) and, finally, a comparison of theoretical and experimental data (section 5).

2. Experimental conditions and theoretical background

Table 1 lists symbols used hereinafter.

2.1 Reagents, chemical and preparation of SAMs at gold electrodes

The relevance of our fitting procedure was tested using two electroactive monolayers (scheme 1). The first monolayer is a TEMPO-based self-assembled monolayer (C15-TEMPO) on a gold substrate, known for its strong attractive interactions between its oxidized species in methylene chloride. The second monolayer is a TTF-based self-assembled monolayer (C12-TTF) on a gold substrate, known for its reversible and sequential oxidation to the corresponding mono- and dicationic forms at moderate potentials in methylene chloride. The synthesis, characterizations, and preparation of C15-TEMPO were described in Ref [14], while the details for C12-TTF can be found in Ref [19]. The gold (Au) substrate consists of a 0.2 cm^2 circular disc comprising an initial adhesion layer of chromium, with a thickness of 2 nm, followed by a 35 nm layer of gold. Both of these layers are deposited onto a glass substrate using the process of physical vapor deposition. (10^{-6} mbar).

2.2. Electrochemical measurements

Conventional cyclic voltammetry (CV) experiments were conducted using a Biologic SP-300 potentiostat controlled by the EC-Lab software, incorporating ohmic drop compensation (resistance is measured using impedance spectroscopy at a frequency of 100 kHz and is real-time hardware-compensated to 85% of the measured value). The experiments were performed in a three-electrode cell maintained at a temperature of 293 K within an argon-filled glove box, ensuring dryness and oxygen-free conditions (< 1 ppm). The working electrodes consisted of an Au-SAM surface, while platinum wires served as counter electrodes. For accurate potential measurements, either Ag wire or $Ag/AgNO_3$ (0.01 M CH_3CN) were used as reference electrodes. The choice of reference electrode enabled precise potential determination. The experiments were carried out in dry HPLC-grade methylene chloride with the addition of tetrabutylammonium hexafluorophosphate (Bu_4NPF_6, electrochemical grade, Fluka) as the supporting electrolyte.

In a cyclic voltammetry experiment, the charge (Q) associated with the process is determined by integrating the voltametric signal. The surface coverage (Γ) of the electroactive species on the

electrode surface can then be calculated using $\Gamma = Q / (n F A)$. Here, n is the number of electrons involved in the redox process, F is the Faraday constant, and A is the active surface area of the electrode (assumed to be equivalent to the macroscopic geometric area, i.e., implying a highly smooth surface). This equation establishes a relationship between the charge passed during the electrochemical process and the extent of surface coverage of the electroactive species on the electrode surface.

2.3. Generation of simulated voltammograms

As previously reported [15,20], to ensure direct comparability with previous studies, all simulated cyclic voltammograms (CVs) were generated using Python 3.11 and/or MATLAB R2020b software running on a conventional desktop computer. A rudimentary numerical method was employed, mimicking a real experiment by approximating the continuous change of the applied potential as a sequence of potential steps ΔE over a time interval Δt. By using a sufficiently small increment ΔE (at least 1 mV), it is reasonable to assume that the oxidation (k_{ox}) and reduction (k_{red}) rate constants remain quasi-constant during each step. This approach is well-suited to our formalism and can generate any voltammograms regardless of the input parameters (v, $k^{0'}$, a_{ij}, etc.). Particularly in this study, it closely matches theoretical ones under Nernstian conditions.

For a reversible n-electron process involving adsorbed electroactive species described by the Butler-Volmer (BV) kinetic formalism and following to the general lateral interaction model (vide infra), the following set of equations can be employed to simulate CV voltammograms:

$$\begin{cases} O + ne^- \underset{k_{ox}}{\overset{k_{red}}{\rightleftarrows}} R \\ i = nFA\Gamma_{max}\dfrac{d\theta_O}{dt} = nFA\Gamma_{max}\left(k_{ox}\left(\theta - \theta_O\right) - k_{red}\,\theta_O\right) \end{cases} \quad (1)$$

The solution to this first-order differential equation is:

$$\theta_O\left(i+1\right) = \left(\theta_O\left(i\right) - \frac{k_{ox}\left(i+1\right)\theta}{k_{ox}\left(i+1\right) + k_{red}\left(i+1\right)}\right)\exp\left(-\left(k_{ox}\left(i+1\right) + k_{red}\left(i+1\right)\right)\Delta t\right) + \frac{k_{ox}\left(i+1\right)\theta}{k_{ox}\left(i+1\right) + k_{red}\left(i+1\right)}$$

$$\Delta\theta_O = \theta_O\left(i+1\right) - \theta_O\left(i\right) = \left(\frac{k_{ox}\left(i+1\right)\theta}{k_{ox}\left(i+1\right) + k_{red}\left(i+1\right)} - \theta_O\left(i\right)\right)\left(1 - \exp\left(-\left(k_{ox}\left(i+1\right) + k_{red}\left(i+1\right)\right)\Delta t\right)\right) \quad (2)$$

$$\text{with} \begin{cases} \theta_O(i) \text{ the value of } \theta_O \text{ at step } i \\ k_{ox}(i+1) = k_s \exp\left((1-\alpha)\frac{nF}{RT}\left(E(i+1)-E^{0'}\right)\right)\exp\left(-2a_{RR}\frac{\phi(\theta)}{\theta}\theta_R(i)-2a_{OR}\frac{\phi(\theta)}{\theta}\theta_O(i)\right) \\ k_{red}(i+1) = k_s \exp\left(-\alpha\frac{nF}{RT}\left(E(i+1)-E^{0'}\right)\right)\exp\left(-2a_{OO}\frac{\phi(\theta)}{\theta}\theta_O(i)-2a_{OR}\frac{\phi(\theta)}{\theta}\theta_R(i)\right) \\ E(i+1) = \left(E_i + (i+1)\,\Delta t\; v\right) \end{cases}$$

2.4. Procedure of fitting voltammograms

The fitting procedure for voltammograms involved the utilization of the Levenberg-Marquardt algorithm [21,22]. This widely recognized algorithm is an optimization method commonly employed for nonlinear least squares curve fitting. It proves particularly valuable when fitting models to data that may exhibit noisy or inconsistent measurements. The main objective of the algorithm is to determine the model parameters that minimize the sum of squared differences between the model predictions and the observed data. Following the fitting of the function's parameters, they are subsequently utilized to generate a smoothed representation of the adjusted voltammogram.

However, it is important to note that the Levenberg-Marquardt algorithm offers numerous possibilities that require careful fine-tuning to achieve optimal results. The algorithm's flexibility lies in its ability to adapt to various problem settings. It provides options to control convergence criteria, regularization parameters, step size adjustments, and more. Adjusting these options appropriately is crucial to customize the algorithm's behaviour to specific applications and achieve accurate and efficient solutions.

To facilitate users in understanding and applying the Levenberg-Marquardt algorithm, we have included easy-to-understand Python and MATLAB code examples in the Supplementary Information. These code snippets serve as demonstrations of how to utilize the algorithm for fitting cyclic voltammograms. They offer practical illustrations of the algorithm's application and serve as a starting point for researchers and practitioners who wish to incorporate it into their own work.

In the case of recursive functions (*vide infra*), fitting voltammograms requires slightly more computational resources compared to fitting voltammograms based on linear models, as it involves solving a system of nonlinear equations during the fitting process. The time difference amounts to approximately a factor of 10. However, it's important to emphasize that computers are becoming increasingly powerful. As of 2023, computation times for fitting a noisy voltammogram consisting of two waves and a baseline, as depicted in Figure 4, are now less than a tenth of a second. In this scenario, the linear model takes about 0.5 seconds, while the non-linear model demands around 5 seconds of computation time when utilizing a 13th Gen Intel(R) Core(TM) i7-1365U 1.80 GHz processor (HP Elite x360 1040 G10).

3. The GLI model

Our previous work was devoted to theoretical and modelling studies aimed at improving the lateral interaction model proposed by E. LAVIRON [23,24]. Our enhancements involved extending the initial model to account for non-random distributions of electroactive species and considering interactions between redox and non-redox species [25,26]. When focusing on interactions solely between redox species, this model allows for the simulation of current-voltage behaviours and facilitates the extraction of characteristic parameters from CVs obtained under Nernstian conditions from any surface distribution of electroactive monolayers.

To provide a comprehensive summary of the previous works, it is important to outline the main assumptions underlying the generalized lateral interactions (GLI) model. The GLI model can be defined based on the following key assumptions:

- The electroactive species are distributed on a substrate with a unimodal statistical distribution of electroactive neighbours. A parameter $\phi(\theta)$, ranging from 0 to 1 and defined for a normalized surface coverage $\theta = \frac{\Gamma}{\Gamma_{max}}$, quantifies the level of segregation of the electroactive species. For a randomly distributed EM, $\phi(\theta) = \theta$, and when segregation exists on the surface, $\phi(\theta) > \theta$.
- The sum of the normalized surface coverage θ_O and θ_R of oxidized (O) and reduced (R) species is constant and equal to θ.
- The surface occupied by one molecule of O is equal to the surface occupied by one molecule of R.
- The redox reaction is described by Butler-Volmer (BV) kinetic formalism (see 2.3.).
- The electrochemical rate constant of redox adsorbate $k^{0'}$ is independent of the coverage.
- $\mathbf{a_{OO}}$, $\mathbf{a_{RR}}$, and $\mathbf{a_{OR}}$ are the interaction constants between molecules of O, molecules of R, and molecules of O and R, respectively. **a** is positive for attraction and negative for repulsion.

During experiments under Nernstian conditions ($\frac{k^{0'}}{v} \to \infty$), CVs exhibit perfect reversibility, and the current can be expressed [27] as a function of θ_O, the only parameter relating to the progress of the reaction and linked to the potential of the working electrode (E):

$$i(\theta_O) = \frac{n^2F^2Av\Gamma_{max}}{RT}\frac{\theta_O(\theta-\theta_O)\theta}{\theta^2 - 2G\theta_O\phi(\theta)(\theta-\theta_O)} \quad (3)$$

The characteristic parameters of CVs, such as the peak potential (E_p), full width at half maximum (FWHM), and peak current (i_p), can be obtained and defined as follows:

$$E_p(S, \phi(\theta)) = E^{0'} + \frac{RT}{nF}S\phi(\theta) \quad (4)$$

$$FWHM(G, \phi(\theta)) = \frac{2\,RT}{nF}\left[\ln\left(\frac{1+\sqrt{\frac{2-G\phi(\theta)}{4-G\phi(\theta)}}}{1-\sqrt{\frac{2-G\phi(\theta)}{4-G\phi(\theta)}}}\right) - G\phi(\theta)\sqrt{\frac{2-G\phi(\theta)}{4-G\phi(\theta)}}\right] \quad (5)$$

$$i_p(G, \theta, \phi(\theta)) = \frac{n^2F^2vA\,\Gamma_{max}}{RT}\frac{\theta}{2(2-G\phi(\theta))} \quad (6)$$

With n, F, v, A, R, T, E, $E^{0'}$ have their usual meanings (table 1).

$G = a_{OO} + a_{RR} - 2a_{OR} \leq 2$ and $S = a_{RR} - a_{OO}$ are defined as "global interactions" parameters and play a crucial role when associated with $\phi(\theta)$. Specifically, $G\phi(\theta)$ defines the shape of the peak and modulates the FWHM and peak intensity (i_p), while $S\phi(\theta)$ solely determines the position of the peak potential (E_p). $G\phi(\theta)$ and $S\phi(\theta)$ can be seen as global interactions weighted by surface segregation and, consequently, by surface coverage.

4. The rec-GLI function

The GLI model is indeed valuable for predicting important parameters of CVs. However, when it comes to fitting CVs, it becomes necessary to express the current as a function of the applied potential (E), which differs from the expression 1 that was previously expressed as a function of θ_O.

As detailed in our previous work [15], expression 1 becomes:

$$i(X) = \frac{n^2F^2Av\Gamma}{RT}\frac{\exp(X)}{(1+\exp(X))^2 - 2B\exp(X)} \quad (7)$$

$$\text{with}\begin{cases} X = \dfrac{nF}{RT}\left(E - E_p\right) + 2G\dfrac{\phi(\theta)}{\theta}\theta_O - G\phi(\theta) = \dfrac{nF}{RT}\left(E - E_p\right) + 2B\dfrac{\theta_O}{\theta} - B \\ X = \dfrac{nF}{RT}\left(E - E_p\right) + \dfrac{2B}{1+\exp(-X)} - B \end{cases} \quad (8)$$

$$\text{and with}\begin{cases} \dfrac{\theta_O}{\theta} = \dfrac{1}{1+\exp(-X)} \\ B = G\phi(\theta) \text{ and } |B| < 2 \end{cases} \quad (9)$$

The main issue with equation 7 is that the variable X in equation 8 is unmeasurable and defined with both the potential (E) and either (1) the unmeasurable variable θ_O or (2) itself, resulting in recursion. To address this issue, the GLI function was proposed and defined as follows:

$$i(X) = \frac{n^2F^2Av\Gamma}{RT}\frac{\exp(X)}{\left(1+\exp(X)\right)^2 - 2B\exp(X)}$$

$$\text{with}\begin{cases} X = \dfrac{nF}{RT}\left(E - E_p\right) + \dfrac{2B}{1+\exp\left(-\dfrac{nF}{RT}\dfrac{\left(E-E_p\right)}{\left(1-0.4\cdot B\right)}\right)} - B \\ B = G\phi(\theta) \;;\; |B| < 2 \;\;;\;\; \Gamma = \Gamma_{max}\theta \end{cases} \quad (10)$$

And E_p, B and Γ are the unknown parameters of the fit.

However, in the GLI function, an approximation was made for the term X, where the expression (1 - 0.4 B) was used to avoid mathematical recursions induced by interactions. While this approximation helped simplify the calculations, it may have potentially resulted in a loss of precision.

Given this consideration, an interesting question arises: Can we explore and utilize mathematical recursions to our advantage?

If we start again with equation 3, for a full reversible reaction ($\frac{k^{0'}}{v} \to \infty$), the current depends only on θ_O and follows a polynomial relationship. Consequently, it is feasible to express θ_O in terms of the current using the same approach. The initial stage of the process yields a quadratic equation involving variable θ_O, for which the discriminant D is employed to obtain the roots.

$$i(\theta_O) = \frac{n^2F^2Av\Gamma}{RT}\frac{\theta_O(\theta-\theta_O)}{\theta^2-2G\theta_O\phi(\theta)(\theta-\theta_O)} = K\frac{\theta_O(\theta-\theta_O)}{\theta^2-2B\theta_O(\theta-\theta_O)}$$

$$\text{with } \begin{cases} B = G\phi(\theta) \text{ and } |B| < 2 \\ K = \dfrac{n^2F^2Av\Gamma}{RT} \end{cases} \tag{11}$$

$$\theta_O{}^2 - \theta_O\cdot\theta + \frac{i\cdot\theta^2}{2B\cdot i + K} = 0 \qquad D = \theta^2 - \frac{4\cdot i\cdot\theta^2}{2B\cdot i+K} = \theta^2\left(1-\frac{4}{2B+\dfrac{K}{i}}\right) > 0$$

The two roots of the quadratic equation are as follows:

$$\theta_O = \frac{\theta}{2}\cdot\left(1\pm\sqrt{1-\frac{4}{2B+\dfrac{K}{i}}}\right) \qquad \begin{cases} - \text{ in the case of } E < E_p \\ + \text{ in the case of } E > E_p \end{cases} \tag{12}$$

By incorporating this expression into the expression of X (equation 8), it is possible to express X as a function of E and i.

$$X = \frac{nF}{RT}(E-E_p) + 2B\frac{\theta_O}{\theta} - B = \frac{nF}{RT}(E-E_p) \pm B\cdot\sqrt{1-\frac{4}{2B+\dfrac{K}{i}}} \tag{13}$$

$$\text{with } \begin{cases} - \text{ in the case of } E < E_p \\ + \text{ in the case of } E > E_p \end{cases}$$

And lastly, by combining equations 7 and 13, the current (i) becomes a recursive function (rec-GLI function) expressed as a function of itself and the applied potential (E):

$$i(X) = K\frac{\exp(X)}{(1+\exp(X))^2 - 2B\exp(X)} = i(E,i)$$

$$\text{with } \begin{cases} X = \dfrac{nF}{RT}(E-E_p) \pm B\cdot\sqrt{1-\dfrac{4}{2B+\dfrac{K}{i}}} & \begin{cases} - \text{ in the case of } E < E_p \\ + \text{ in the case of } E > E_p \end{cases} \\ B = G\phi(\theta) \;;\; |B| < 2 \;\;;\;\; \Gamma = \Gamma_{max}\theta \\ K = \dfrac{n^2F^2Av\Gamma}{RT} \qquad \text{and} \quad \dfrac{i}{K} = \psi \end{cases} \tag{14}$$

And, as for the GLI function, E_p, B and Γ are the unknown parameters of the rec-GLI function, and the fit conducts to obtain the peak potential $\left\{E_p\ ;\ \sigma_{E_p}\right\}$, the global interaction parameter $\left\{B\ ;\ \sigma_B\right\}$ and the surface coverage $\left\{\Gamma\ ;\ \sigma_\Gamma\right\}$.

One important distinction, when comparing to the GLI function, is that the rec-GLI function i(E, i) incorporates two measurable variables, E and i, without making any approximation in the variable X. Despite the recursive nature of the function with respect to i, this recursion does not pose any obstacle to numerical fitting procedures conducted using Python scripts, MATLAB scripts, or any other programming language.

However, a potential issue that may arise with this type of function is related to measurement errors. In a fitting problem, measurement errors are naturally present in the output variable being adjusted, but they are assumed to be negligible for input variables. In the case of a recursive function, the output variable being adjusted is also an input variable, thereby subject to the same errors, albeit assumed to be negligible. This situation should be thoroughly tested to evaluate the robustness of the function.

Based on the fitted parameters, key characteristic parameters of the CVs (E_p, i_p, and FWHM), along with their corresponding errors, can be determined. Detailed calculations pertaining to these parameters are provided in the Appendix.

Peak potential (E_p) is directly determined by the fit of experimental CVs:

$$\left\{E_p\ ;\ \sigma_{E_p}\right\} \tag{15}$$

Peak intensity (i_p) can be extracted at the maximum of the CV:

$$\begin{aligned} i_p &= i\left(E = E_p \text{ or } X = 0\right) = \frac{n^2F^2Av}{RT}\frac{\Gamma}{4-2B} \\ \sigma_{i_p} &= \frac{n^2F^2Av}{RT}\sqrt{\left(\frac{1}{4-2B}\sigma_\Gamma\right)^2 + \left(\frac{2\Gamma}{(4-2B)^2}\sigma_B\right)^2} \end{aligned} \tag{16}$$

FWHM is calculated at i_p / 2:

$$\mathrm{FWHM} = 2\frac{RT}{nF}\left(\ln\left(\frac{1+\sqrt{\frac{(B-2)}{(B-4)}}}{1-\sqrt{\frac{(B-2)}{(B-4)}}} \right) - B\sqrt{\frac{(B-2)}{(B-4)}} \right) \qquad (17)$$

$$\sigma_{\mathrm{FWHM}} = 2\frac{RT}{nF}\left(\frac{(B-2)(B-6)}{(B-4)^2\sqrt{\frac{(B-2)}{(B-4)}}} \right)\sigma_B$$

Hence, all the characteristic parameters of the CVs and their corresponding errors are determined based on the fitted parameters.

5. Results and discussions

5.1. rec-GLI function vs. GLI function (interaction conditions)

To evaluate the accuracy of the rec-GLI function under controlled conditions, we conducted a simulation of cyclic voltammograms (CVs) for three specific values of the G and S parameters (G = -S = +1 ; 0 ; -1) with initial conditions chosen as $\theta = 1 = \phi(\theta)$ and {n = 1, $k^{0'}$ = 1000 s^{-1}, v = 0.1 $V.s^{-1}$, $E^{0'}$ = 0 V, T = 293 K, A = 0.2 cm^2 and Γ_{max} = 5 10^{-10} $mol.cm^{-2}$}. We chose G = -S because this case artificially enforces the presence of interactions solely among the oxidized species ($a_{OO} \neq 0$), a quite common experimental scenario. The simulated CVs were then fitted, with the procedure describe in section 2.4., with the rec-GLI function and the GLI function to obtain characteristic parameters such as Γ, B, E_p, i_p and FWHM.

The obtained fitting results (figure 1, table 2 and ref. [15]) clearly demonstrate that, overall, the rec-GLI function outperforms the GLI function in terms of accuracy (Δ) and precision (Sx), even though the latter remains quite close in terms of results despite the approximation used.

In all the investigated cases, it is important to note that absolute variations $\Delta = |\mathrm{theoretical} - \mathrm{fitted}|$, and standard deviations (Sx) consistently show lower values with the rec-GLI function, indicating higher fidelity and improved accuracy of the fitting procedure. Additionally, commonly used criteria for evaluating the quality of a fit, such as residual analysis ($i_{residual} = i_{simulated} - i_{fitted}$) presented in figure

1, as well as statistical indicators like RMS error, chi-squared (χ^2), and coefficient of determination (R^2), consistently favour the rec-GLI function.

Another significant advantage of the rec-GLI function is observed in less restrictive cases, where broad voltammograms are obtained ($G < 0$). In such cases, the absolute variations are lower than the standard deviations (i.e., $\Delta < Sx$), indicating that the adjusted values consistently fall within the statistical confidence intervals (95%). However, it is worth noting that the determination of E_p is influenced by the step size used in the simulation and is subject to systematic errors, therefore $\Delta(E_p)$ is just a rough estimate.

Conversely, in more restrictive cases resulting in narrow voltammograms ($G > 0$), the potential step size not only affects the determination of E_p but also the other parameters, leading to absolute variations larger than standard deviations. Consequently, the adjusted values may fall outside the statistical confidence intervals (95%). Taking into account the errors introduced during the modelling process (section 2.3.), the fitting procedure using the rec-GLI function allows accurate parameter estimation for the studied voltammograms. This contrasts with previous studies that reported sharp peaks and discontinuities.

Lastly, it is important to highlight that when $B = 0$ (representing the ideal case without interaction), the rec-GLI function simplifies to the LAVIRON case [24]. In other words, the ideal case inherently corresponds to a specific instance of the rec-GLI function. As expected, the fitting procedure yields excellent results in this case, with standard deviations lower than 10^{-9}.

The study across all cases provides compelling evidence for the effectiveness of the rec-GLI function in accurately fitting simulated cyclic voltammograms under well-controlled conditions.

5.2. rec-GLI function vs. Generalized Lateral Interactions model

To further validate the reliability of the rec-GLI function in controlled conditions, a series of cyclic voltammograms (CVs) based on the GLI model were simulated for various cases involving phase segregation ($\phi(\theta) > \theta$). Specifically, simulations were performed using a challenging value of the G

parameter (G > 0; G = -S = +1) and with fixed experimental conditions {n = 1, $k^{0'}$ = 1000 s^{-1}, v = 0.1 $V.s^{-1}$, $E^{0'}$ = 0 V, T = 293 K, A = 0.2 cm^2 and Γ_{max} = 5 10^{-10} $mol.cm^{-2}$}. The simulated CVs were then fitted using the rec-GLI function to extract characteristic parameters including E_p, i_p, FWHM, Γ, and B. These parameters were subsequently plotted against the theoretical surface coverage Γ (figure 2) and compared to the expected values derived from the GLI model. As expected, the agreement observed between the simulated voltammograms and the fitted voltammograms serves as evidence for the effectiveness of the rec-GLI function (all error bars are included within the plotted points), except for the parameter E_p, which deviates when peaks are weak as Γ approaches Γ_{max} as previously noted.

Across a wide range of surface coverage and phase segregation, all characteristic parameters exhibit a good fit with their corresponding theoretical values [26].

5.3. rec-GLI function (gaussian noisy case)

To assess the impact of noisy conditions on cyclic voltammograms (CVs), we performed simulations by introducing a substantial level of Gaussian noise (σ_{noise}= 0.5 µA) to the simulated CV. The initial conditions chosen are G = -S = +0.85, $\theta = 0.75 = \phi(\theta)$ and {n = 1, $k^{0'}$ = 1000 s^{-1}, v = 0.1 $V.s^{-1}$, $E^{0'}$ = 0 V, T = 293 K, A = 0.2 cm^2 and Γ_{max} = 5 10^{-10} $mol.cm^{-2}$}.

Given that the function rec-GLI is recursive on the current, the fitting procedure will inevitably be affected by the measurement noise of this same current (equation 14). Figure 3A shows that the fit (red line) remains very comparable and of the same quality as the fit performed with the GLI function (figure 3C).

Despite the measurement noise, which typically affects the fit due to recursion, the obtained fitting parameters (table 3) are very close to the theoretical values and consistently show improvement with the rec-GLI function compared to the GLI function in terms of accuracy (Δ) and precision (Sx).

The plotted residual errors, calculated with the simulated noise-free CV for better readability, are of the same order of magnitude despite the inherent noise introduced by reusing the noisy initial current

for the calculation of the fitted current (equation 14). To overcome this recursion noise and to visually confirm the high accuracy of the characteristic parameters in the fitted CVs, an approximate simulation of the CVs can be carried out using an algorithm based on the Newton-Raphson method [28]. It is well known that this method employs an iterative numerical technique to yield rough solutions for equations, specifically focusing on the roots of real-valued functions. It serves as a robust and extensively utilized approach for solving equations in situations where obtaining analytical solutions is challenging or not possible, as is the case with the GLI function.

Consequently, by employing the definition of the GLI function and integrating the fitted parameters, it becomes feasible to generate an approximate simulation of the current that is devoid of noise and follows a monotonic pattern. With this calculation procedure, residual errors are smoothed (figure 3B) and are two times lower than those of the GLI function, demonstrating the reliability of the obtained fitting parameters.

5.4. rec-GLI function vs. experimental voltammograms

After the successful validation using simulated cyclic voltammograms (CVs), the next phase involves the experimental assessment of the rec-GLI function. This evaluation specifically targets two widely studied redox-responsive materials: self-assembled monolayers (SAMs) based on TEMPO and TTF moieties (scheme 1).

At this stage, it is important to note that to account for the unpredictable fluctuations observed in the baseline of the experimental cyclic voltammogram (CV), a monotonic fourth-order polynomial function, denoted as $g(x) = \pm\sum_{i=0}^{n}\left|a_i.x^i\right|$, is introduced and incorporated into the fitting functions. The primary objective of this approach is to improve the accuracy and reliability of the curve-fitting process [15].

TEMPO-based self-assembled monolayers undergo a reversible one-electron oxidation process in both non-aqueous and aqueous solvents. The shape of the cyclic voltammetry peak is influenced by

the interactions among its oxidized species, which can be either attractive or repulsive depending on solvents used. In the presence of 0.1M $TBAPF_6/CH_2Cl_2$, attractive interactions prevail, resulting in the generation of sharp peak cyclic voltammograms. This characteristic poses a challenge when applying the rec-GLI function and figure 4A demonstrates the suitability of the rec-GLI function for accurately fitting the experimental curve, particularly in the proximity of the peak potential. This enables the accurate determination of characteristic parameters of the cyclic voltammograms (CVs) with significant precision. Moreover, the rec-GLI function exhibited outstanding fitting performance for voltammetric responses in both water (FWHM = 90 mV) and acetonitrile, where the resulting voltammetric peaks displayed broader widths (FWHM > 90 mV). These results, when compared to previous studies [15,29], exhibit similar magnitudes but showcase enhanced accuracy.

TTF-based SAMs undergo reversible and sequential oxidation processes in 0.1M $TBAPF_6/CH_2Cl_2$, leading to the formation of mono- and dicationic forms. Importantly, these redox reactions remain unaffected by the substitution of hydrogen atoms on the TTF core with different functional groups and the width of the redox waves observed in CVs is strongly influenced by the oxidation states of the TTF moieties, primarily due to intermolecular interactions [30]. To evaluate the suitability of the rec-GLI function for TTF-based SAMs, it is necessary to ensure the conservation of charges during the two consecutive oxidation processes. This constraint is integrated into the fitting procedure by enforcing equal surface coverages ($\Gamma_1 = \Gamma_2 = \Gamma$) to achieve an accurate alignment between the model and the experimental data. Figure 4B demonstrates the ability of the rec-GLI function to extract the parameters E_p, i_p, FWHM, Γ, and B from a partially covered TTF-based SAM on Au substrate, despite the presence of measurement noise, significant baseline drift and both broad and narrow peaks.

Finally, it should be noted that the effectiveness of the rec-GLI function has also been successfully tested on other redox materials, including Bithiophene-based SAMs [31], Ferrocene-based SAMs [32,33], and Perylenediimide-based SAMs [34].

6. Conclusion

In conclusion, this work introduces the rec-GLI function as an innovative mathematical tool for accurately fitting cyclic voltammograms (CVs) and estimating lateral interaction parameters on electroactive monolayers or redox responsive materials. By incorporating mathematical recursion and advanced curve fitting algorithms, the rec-GLI function exhibits enhanced accuracy in parameter estimation compared to existing models, particularly in cases of strong interactions ($B > 0$), making it closer to theoretical predictions and outperforming the empirical GLI function.

The successful application of the rec-GLI function in fitting CVs of TEMPO-, TTF- and many other-based SAMs on Au substrates highlights its effectiveness, and the Levenberg-Marquardt algorithm enables robust solutions in the presence of noise or inconsistent measurements.

Overall, the introduction of the rec-GLI function offers a reliable mathematical framework for studying the redox behaviour of electroactive monolayers and estimating lateral interaction parameters.

Acknowledgments

The authors thank Flavy ALEVEQUE for her critical reading of the manuscript, Dr. Christelle GAUTIER for the synthesis of TEMPO-based molecules and the plateau CARMA of the SFR MATRIX (University of ANGERS) for the electrochemical characterizations.

References

[1] W.C. Bigelow, D.L. Pickett, W.A. Zisman, Oleophobic monolayers: I. Films adsorbed from solution in non-polar liquids, J. Colloid Sci. 1 (1946) 513–538. https://doi.org/10.1016/0095-8522(46)90059-1.

[2] J.C. Love, L.A. Estroff, J.K. Kriebel, R.G. Nuzzo, G.M. Whitesides, Self-Assembled Monolayers of Thiolates on Metals as a Form of Nanotechnology, Chem. Rev. 105 (2005) 1103–1170. https://doi.org/10.1021/cr0300789.

[3] L. Srisombat, A.C. Jamison, T.R. Lee, Stability: A key issue for self-assembled monolayers on gold as thin-film coatings and nanoparticle protectants, Colloids Surf. Physicochem. Eng. Asp. 390 (2011) 1–19. https://doi.org/10.1016/j.colsurfa.2011.09.020.

[4] D. Marchi, E. Cara, F.F. Lupi, P. Hönicke, Y. Kayser, B. Beckhof, M. Castellino, P. Klapetek, A. Zoccante, M. Laus, M. Cossi, Structure and stability of 7-mercapto-4-methylcoumarin self-assembled monolayers on gold: an experimental and computational analysis, Phys. Chem. Chem. Phys. 24 (2022) 22083–22090. https://doi.org/10.1039/D2CP03103E.

[5] M. Delamar, R. Hitmi, J. Pinson, J.M. Saveant, Covalent modification of carbon surfaces by grafting of functionalized aryl radicals produced from electrochemical reduction of diazonium salts, J. Am. Chem. Soc. 114 (1992) 5883–5884. https://doi.org/10.1021/ja00040a074.

[6] V. Shkirskiy, E. Levillain, C. Gautier, Capacitive Impedance for Following In-Situ Grafting Kinetics of Diazonium Salts, ChemPhysChem. 22 (2021) 1074–1078. https://doi.org/10.1002/cphc.202100154.

[7] C. Combellas, F. Kanoufi, J. Pinson, F.I. Podvorica, Sterically Hindered Diazonium Salts for the Grafting of a Monolayer on Metals, J. Am. Chem. Soc. 130 (2008) 8576–8577. https://doi.org/10.1021/ja8018912.

[8] A.L. Eckermann, D.J. Feld, J.A. Shaw, T.J. Meade, Electrochemistry of redox-active self-assembled monolayers, Coord. Chem. Rev. 254 (2010) 1769–1802. https://doi.org/10.1016/j.ccr.2009.12.023.

[9] A.J. Bard, L.R. Faulkner, Electrochemical Methods: Fundamentals and Applications, 2nd Edition, John Wiley & Sons, New York, 2001.

[10] J.J. Calvente, R. Andreu, Intermolecular interactions in electroactive thiol monolayers probed by linear scan voltammetry, Curr. Opin. Electrochem. 1 (2017) 22–26. https://doi.org/10.1016/j.coelec.2016.12.006.

[11] J. González, J.-A. Sequí, Analysis of the Electrochemical Response of Surface-confined Bidirectional Molecular Electrocatalysts in the Presence of Intermolecular Interactions, ChemCatChem. 13 (2021) 747–762. https://doi.org/10.1002/cctc.202001599.

[12] J. Gonzalez, J.-A. Sequí, Square Wave Voltcoulommetry Analysis of the Influence of the Electrostatic Environment on the Electrochemical Functionality of Redox Monolayers, ChemElectroChem. 6 (2019) 2290–2301. https://doi.org/10.1002/celc.201900352.

[13] J.V. Hernandez-Tovar, M. López-Tenés, J. Gonzalez, Square Wave Voltcoulommetry of two-electron molecular electrocatalytic processes with adsorbed species. Application to the surface O2 reduction in acetonitrile at anthraquinone-modified glassy carbon electrodes, Electrochimica Acta. 444 (2023) 142000. https://doi.org/10.1016/j.electacta.2023.142000.

[14] O. Aleveque, F. Seladji, C. Gautier, M. Dias, T. Breton, E. Levillain, Nitroxyl Radical Self-Assembled Monolayers on Gold: Versatile Electroactive Centers in Aqueous and Organic Media, Chemphyschem. 10 (2009) 2401–2404. https://doi.org/10.1002/cphc.200900448.

[15] O. Alévêque, E. Levillain, A generalized lateral interactions function to fit voltammetric peaks of self-assembled monolayers, Electrochem. Commun. 67 (2016) 73–79. https://doi.org/10.1016/j.elecom.2016.04.003.

[16] V.D. Ivanov, Adsorption voltammetric peak: approximate calculation algorithm taking into account lateral interactions, J. Solid State Electrochem. 23 (2019) 1371–1377. https://doi.org/10.1007/s10008-019-04235-3.

[17] J. Waelder, S. Maldonado, Beyond the Laviron Method: A New Mathematical Treatment for Analyzing the Faradaic Current in Reversible, Quasi-Reversible, and Irreversible Cyclic Voltammetry of Adsorbed Redox Species, Anal. Chem. 93 (2021) 12672–12681. https://doi.org/10.1021/acs.analchem.1c02503.
[18] R. Vasquez, J. Waelder, Y. Liu, H. Bartels, S. Maldonado, A Gauss's law analysis of redox active adsorbates on semiconductor electrodes: The charging and faradaic currents are not independent, Proc. Natl. Acad. Sci. 119 (2022) e2202395119. https://doi.org/10.1073/pnas.2202395119.
[19] P.Y. Blanchard, O. Aleveque, S. Boisard, C. Gautier, A. El-Ghayoury, F. Le Derf, T. Breton, E. Levillain, Intermolecular interactions in self-assembled monolayers of tetrathiafulvalene derivatives, Phys. Chem. Chem. Phys. 13 (2011) 2118–2120. https://doi.org/10.1039/c0cp01968b.
[20] O. Alévêque, E. Levillain, Use of phase angle in alternating voltammetry on redox self-assembled monolayers with intermolecular interactions, J. Electroanal. Chem. 925 (2022) 116914. https://doi.org/10.1016/j.jelechem.2022.116914.
[21] K. Levenberg, A method for the solution of certain non-linear problems in least squares, Q. Appl. Math. 2 (1944) 164–168. https://doi.org/10.1090/qam/10666.
[22] D.W. Marquardt, An Algorithm for Least-Squares Estimation of Nonlinear Parameters, J. Soc. Ind. Appl. Math. 11 (1963) 431–441. https://doi.org/10.1137/0111030.
[23] E. Laviron, Surface linear potential sweep voltammetry: Equation of the peaks for a reversible reaction when interactions between the adsorbed molecules are taken into account, J. Electroanal. Chem. Interfacial Electrochem. 52 (1974) 395–402. https://doi.org/10.1016/S0022-0728(74)80449-3.
[24] E. Laviron, L. Roullier, General expression of the linear potential sweep voltammogram for a surface redox reaction with interactions between the adsorbed molecules: Applications to modified electrodes, J. Electroanal. Chem. Interfacial Electrochem. 115 (1980) 65–74. https://doi.org/10.1016/S0022-0728(80)80496-7.
[25] O. Alévêque, E. Levillain, Electroactive mixed self-assembled monolayers: Lateral interactions model updated to interactions between redox and non-redox species, Electrochem. Commun. 34 (2013) 165–169. https://doi.org/10.1016/j.elecom.2013.06.009.
[26] O. Alévêque, P.-Y. Blanchard, C. Gautier, M. Dias, T. Breton, E. Levillain, Electroactive self-assembled monolayers: Laviron's interaction model extended to non-random distribution of redox centers, Electrochem. Commun. 12 (2010) 1462–1466. https://doi.org/10.1016/j.elecom.2010.07.039.
[27] O. Aleveque, P.Y. Blanchard, C. Gautier, M. Dias, T. Breton, E. Levillain, Electroactive self-assembled monolayers: Laviron's interaction model extended to non-random distribution of redox centers, Electrochem. Commun. 12 (2010) 1462–1466. https://doi.org/10.1016/j.elecom.2010.07.039.

Appendix

To determine the standard deviations of the parameters of interest in this appendix, the standard formula utilized by engineers and experimental scientists to calculate statistical standard deviation through variance propagation is as follows:

$$\sigma_f = \sqrt{\sigma_x^2 \left(\frac{\partial f(x,y,...)}{\partial x} \right)^2 + \sigma_y^2 \left(\frac{\partial f(x,y,...)}{\partial y} \right)^2 + ...}$$

Where σ_f denotes the standard deviation of the function f(x, y, ...), σ_x stands for the standard deviation of x, σ_y corresponds to the standard deviation of y, and so on.

*****

Peak potential (E_p) is directly determined by the fit of experimental CVs:

$$E_p \pm \sigma_{E_p}$$

*****

Peak intensity (i_p) can be extracted at the maximum of the CV, i.e., when the derivative of i is zero.

$$i(X) = K \frac{\exp(X)}{(1+\exp(X))^2 - 2B\exp(X)}$$

$$\frac{di}{dX} = K \frac{\exp(X) \cdot (\exp(2X) - 1)}{(2B \cdot \exp(X) - \exp(2X) - 2 \cdot \exp(X) - 1)^2}$$

$$\frac{di}{dX} = 0 \quad \Rightarrow \quad X = 0 \quad \text{and} \quad X = \frac{nF}{RT}(E - E_p) + \frac{2B}{1+\exp(0)} - B = 0 \quad \Rightarrow \quad E = E_p$$

$$i_p = i(E = E_p \text{ or } X = 0) = K \frac{\Gamma}{4-2B} = \frac{n^2F^2Av}{RT} \frac{\Gamma}{4-2B}$$

$$\sigma_{i_p} = \frac{n^2F^2Av}{RT} \sqrt{\left(\frac{1}{4-2B} \sigma_\Gamma \right)^2 + \left(\frac{2\Gamma}{(4-2B)^2} \sigma_B \right)^2}$$

*****

FWHM is calculated at $i_p/2$:

$$i_{FWHM} = \frac{i_p}{2} = \frac{n^2F^2Av}{RT}\frac{\Gamma}{2(4-2B)} = \frac{K}{2(4-2B)}$$

$$i_{FWHM}(Z) = K\frac{Z}{(1+Z)^2-2BZ} \quad \text{with} \quad Z = \exp(X) \Leftrightarrow X = \ln(Z)$$

$$\frac{K}{2(4-2B)} = K\frac{Z}{(1+Z)^2-2BZ}$$

$$(1+Z)^2-2BZ = 2Z(4-2B)$$

$$Z^2+(2B-6)Z+1=0$$

$$\Delta = (2B-6)^2-4 = 4(B^2-6B+8) = 4(B-2)(B-4)$$

$$Z = \frac{-(2B-6)\pm\sqrt{4(B-2)(B-4)}}{2}$$

$$Z = \frac{-((B-2)+(B-4))\pm\sqrt{4(B-2)(B-4)}}{2}$$

$$Z = \frac{-1-\frac{(B-2)}{(B-4)}\pm 2\sqrt{\frac{(B-2)}{(B-4)}}}{\frac{2}{(B-4)}}$$

Note that since B < 2, the expressions (B-4) and (B-2) are negative.

$$Z^- = \frac{-1-\frac{(B-2)}{(B-4)}+2\sqrt{\frac{(B-2)}{(B-4)}}}{\frac{2}{(B-4)}} \quad \text{and with} \quad -(a^2-2ab+b^2) = -(a-b)^2$$

$$Z^- = \frac{\left(1-\sqrt{\frac{(B-2)}{(B-4)}}\right)^2}{-\frac{2}{(B-4)}}$$

$$Z^+ = \frac{-1-\frac{(B-2)}{(B-4)}-2\sqrt{\frac{(B-2)}{(B-4)}}}{\frac{2}{(B-4)}} \quad \text{and with} \quad -(a^2+2ab+b^2) = -(a+b)^2$$

$$Z^{+} = \frac{\left(1+\sqrt{\frac{(B-2)}{(B-4)}}\right)^{2}}{-\frac{2}{(B-4)}}$$

Note that Z^{+} and Z^{-} are interconnected values:

$$Z^{+}\cdot Z^{-} = \frac{\left(1+\sqrt{\frac{(B-2)}{(B-4)}}\right)^{2}}{-\frac{2}{(B-4)}} \cdot \frac{\left(1-\sqrt{\frac{(B-2)}{(B-4)}}\right)^{2}}{-\frac{2}{(B-4)}}$$

$$Z^{+}\cdot Z^{-} = \left(\frac{\left(1+\sqrt{\frac{(B-2)}{(B-4)}}\right)\left(1-\sqrt{\frac{(B-2)}{(B-4)}}\right)}{-\frac{2}{(B-4)}}\right)^{2} = \left(\frac{\left(1^{2}-\frac{(B-2)}{(B-4)}\right)}{-\frac{2}{(B-4)}}\right)^{2}$$

$$Z^{+}\cdot Z^{-} = \left(\frac{\left((B-4)-(B-2)\right)}{-2}\right)^{2} = 1$$

And then $Z^{+} = \frac{1}{Z^{-}} \rightarrow \ln\left(Z^{+}\right) = \ln\left(\frac{1}{Z^{-}}\right) = -\ln\left(Z^{-}\right) \rightarrow X^{+} = -X^{-}$

FWHM is defined as:

$$FWHM = E^{+} - E^{-}$$

With

$$X = \frac{nF}{RT}\left(E - E_{p}\right) + 2B\frac{\theta_{O}}{\theta} - B \;\rightarrow\; E = E_{p} + \frac{RT}{nF}\left(X - 2B\frac{\theta_{O}}{\theta} + B\right)$$

With $\frac{\theta_{O}}{\theta} = \frac{1}{1+\exp(-X)}$

$$FWHM = E^{+} - E^{-} = \frac{RT}{nF}\left(\left(X^{+} - X^{-}\right) - 2B\left(\frac{1}{1+\exp(-X^{+})} - \frac{1}{1+\exp(-X^{-})}\right)\right)$$

And with $Z = \exp(X)$ and thus $\frac{1}{Z} = \exp(-X)$

$$\mathrm{FWHM} = \mathrm{E}^+ - \mathrm{E}^- = \frac{\mathrm{RT}}{\mathrm{nF}}\left(\left(\mathrm{X}^+ - \mathrm{X}^-\right) - 2\mathrm{B}\left(\frac{1}{1+1/\mathrm{Z}^+} - \frac{1}{1+1/\mathrm{Z}^-)}\right)\right)$$

Part 1: $\left(\mathrm{X}^+ - \mathrm{X}^-\right)$

$$\mathrm{X}^+ - \mathrm{X}^- = \ln(\mathrm{Z}^+) - \ln(\mathrm{Z}^-) = \ln\left(\frac{\mathrm{Z}^+}{\mathrm{Z}^-}\right)$$

$$\mathrm{X}^+ - \mathrm{X}^- = \ln\left(\frac{\left(1+\sqrt{\frac{(\mathrm{B}-2)}{(\mathrm{B}-4)}}\right)^2}{\left(1-\sqrt{\frac{(\mathrm{B}-2)}{(\mathrm{B}-4)}}\right)^2}\right) = 2\ln\left(\frac{1+\sqrt{\frac{(\mathrm{B}-2)}{(\mathrm{B}-4)}}}{1-\sqrt{\frac{(\mathrm{B}-2)}{(\mathrm{B}-4)}}}\right)$$

Part 2: $\left(\frac{1}{1+1/\mathrm{Z}^+} - \frac{1}{1+1/\mathrm{Z}^-)}\right)$

$$\frac{1}{1+1/\mathrm{Z}^+} - \frac{1}{1+1/\mathrm{Z}^-} = \frac{1}{1+1/\mathrm{Z}^+} - \frac{1}{1+\mathrm{Z}^+} = -\frac{1-\mathrm{Z}^+}{1+\mathrm{Z}^+}$$

$$= -\frac{-\frac{2}{(\mathrm{B}-4)} - \left(1+\sqrt{\frac{(\mathrm{B}-2)}{(\mathrm{B}-4)}}\right)^2}{-\frac{2}{(\mathrm{B}-4)} + \left(1+\sqrt{\frac{(\mathrm{B}-2)}{(\mathrm{B}-4)}}\right)^2} = -\frac{-\frac{2}{(\mathrm{B}-4)} - \left(1+2\sqrt{\frac{(\mathrm{B}-2)}{(\mathrm{B}-4)}}+\frac{(\mathrm{B}-2)}{(\mathrm{B}-4)}\right)}{-\frac{2}{(\mathrm{B}-4)} + \left(1+2\sqrt{\frac{(\mathrm{B}-2)}{(\mathrm{B}-4)}}+\frac{(\mathrm{B}-2)}{(\mathrm{B}-4)}\right)}$$

$$= -\frac{-\frac{2}{(\mathrm{B}-4)} - \left(\frac{(\mathrm{B}-4)}{(\mathrm{B}-4)}+2\sqrt{\frac{(\mathrm{B}-2)}{(\mathrm{B}-4)}}+\frac{(\mathrm{B}-2)}{(\mathrm{B}-4)}\right)}{-\frac{2}{(\mathrm{B}-4)} + \left(\frac{(\mathrm{B}-4)}{(\mathrm{B}-4)}+2\sqrt{\frac{(\mathrm{B}-2)}{(\mathrm{B}-4)}}+\frac{(\mathrm{B}-2)}{(\mathrm{B}-4)}\right)} = -\frac{\frac{-2\mathrm{B}+4}{(\mathrm{B}-4)} - 2\sqrt{\frac{(\mathrm{B}-2)}{(\mathrm{B}-4)}}}{\frac{2\mathrm{B}-8}{(\mathrm{B}-4)} + 2\sqrt{\frac{(\mathrm{B}-2)}{(\mathrm{B}-4)}}}$$

$$= -\frac{\frac{-2(\mathrm{B}-2)}{(\mathrm{B}-4)} - 2\sqrt{\frac{(\mathrm{B}-2)}{(\mathrm{B}-4)}}}{2+2\sqrt{\frac{(\mathrm{B}-2)}{(\mathrm{B}-4)}}} = -\frac{-2\cdot\sqrt{\frac{(\mathrm{B}-2)}{(\mathrm{B}-4)}}\left(\sqrt{\frac{(\mathrm{B}-2)}{(\mathrm{B}-4)}}+1\right)}{2\cdot\left(\sqrt{\frac{(\mathrm{B}-2)}{(\mathrm{B}-4)}}+1\right)} = \sqrt{\frac{(\mathrm{B}-2)}{(\mathrm{B}-4)}}$$

Part1 and Part2 combined:

$$\mathrm{FWHM} = \mathrm{E}^+ - \mathrm{E}^- = \frac{\mathrm{RT}}{\mathrm{nF}}\left(\left(\mathrm{X}^+ - \mathrm{X}^-\right) - 2\mathrm{B}\left(\frac{1}{1+1/\mathrm{Z}^+} - \frac{1}{1+1/\mathrm{Z}^-)}\right)\right)$$

$$\mathrm{FWHM} = 2\frac{\mathrm{RT}}{\mathrm{nF}}\left(\ln\left(\frac{1+\sqrt{\frac{(\mathrm{B}-2)}{(\mathrm{B}-4)}}}{1-\sqrt{\frac{(\mathrm{B}-2)}{(\mathrm{B}-4)}}}\right) - \mathrm{B}\sqrt{\frac{(\mathrm{B}-2)}{(\mathrm{B}-4)}}\right)$$

$$\sigma_{FWHM} = 2\frac{RT}{nF}\left(\frac{(B-2)(B-6)}{(B-4)^2\sqrt{\frac{(B-2)}{(B-4)}}}\right)\sigma_B$$

Recursive Function for Fitting Electroactive Monolayer Cyclic Voltammograms and Extracting Key Parameters

Olivier Alévêque and Eric Levillain

Univ Angers, CNRS, MOLTECH-ANJOU, SFR MATRIX, F-49000 Angers, France

Corresponding authors:

olivier.aleveque@univ-angers.fr (Olivier ALEVEQUE)

Tel.: (+33)241735090; Fax: (+33)241735405

eric.levillain@univ-angers.fr (Eric LEVILLAIN)

Tel.: (+33)241735095; Fax: (+33)241735405

TABLES

Table 1: Major symbols and definitions used in this work

Symbol	Units	Description
E	V	Applied potential
i	A	Measured current
t	s	Acquisition time
$E^{0'}$	V	Apparent standard potential of redox adsorbate
$k^{0'}$	s^{-1}	Standard rate constant of redox adsorbate
k_{ox} , k_{red}	s^{-1}	Oxidation and reduction rate constants
α		Charge-transfer coefficient
FWHM	V	Full Width at Half Maximum
Ep	V	Peak potential
ip	A	Peak intensity
Cdl	F	Double layer capacity
v	$V.s^{-1}$	Scan rate
Q	C	Electrical charge involved in the redox process
n		Number of electrons involved in the redox process
F	$C.mol^{-1}$	Faraday constant
A	cm^2	Active surface area
R	$J{\cdot}K^{-1}{\cdot}mol^{-1}$	Molar gas constant
T	K	Temperature
Γ	$mol.cm^{-2}$	Surface coverage of electroactive species
Γ_{max}	$mol.cm^{-2}$	Maximum surface coverage of electroactive species
$\theta = \frac{\Gamma}{\Gamma_{max}}$		Normalized surface coverage of electroactive species
$\phi(\theta)$		Segregation constant ($\theta < \phi(\theta) < 1$)
θ_O		Normalized surface coverage of oxidized species
θ_R		Normalized surface coverage of reduced species
a_{ij}		Interaction constant between immobilized molecules i and j represent oxidized or reduced species
G , S		Global interaction parameters depending on a_{ij}

Table 2: Results of the fitting processes ($\frac{k}{v} \to \infty$, n = 1, k_0 = 1000 s^{-1}, v = 0.1 $V.s^{-1}$, E^0= 0 V, T = 293 K, A = 0.2 cm^2 and Γ_{max} = 5 10^{-10} $mol.cm^{-2}$) in the case of G = -S = {+1 ; 0 ; -1} and $\theta = 1 = \phi(\theta)$

Condition	Parameters	Simulated	GLI Function	rec-GLI Function
G = -S = +1 $\theta = 1 = \phi(\theta)$	Ep vs E^0 (V) *	- 0.025249	-0.024282 *Δ = 0.000967* *Sx = 0.000017*	- 0.024331 *Δ = 0.000918* *Sx = 0.000015*
	B	1	1.0125 *Δ = 0.0125* *Sx = 0.0015*	0.9923 *Δ = 0.0077* *Sx = 0.0012*
	Γ (10^{-10} mol.cm^{-2})	5	4.8842 *Δ = 0.1158* *Sx = 0.0057*	5.0126 *Δ = 0.0126* *Sx = 0.0044*
	Ip (µA)	19.107	18.900 *Δ = 0.207* *Sx = 0.035*	19.008 *Δ = 0.099* *Sx = 0.028*
	FWHM (V)	0.037348	0.039353 *Δ = 0.002005* *Sx = 0.000064*	0.037725 *Δ = 0.000377* *Sx = 0.000059*
G = -S = 0 $\theta = 1 = \phi(\theta)$	Ep vs E^0 (V) *	0	- 0.00050 *Sx < 10^{-9}*	- 0.00049 *Sx < 10^{-9}*
	B	0	- 0.000066 *Sx < 10^{-9}*	- 0.000066 *Sx < 10^{-9}*
	Γ (10^{-10} mol.cm^{-2})	5	4.99999 *Sx < 10^{-9}*	4.99999 *Sx < 10^{-9}*
	ip (µA)	9.55346	9.55315 *Sx < 10^{-14}*	9.55315 *Sx < 10^{-14}*
	FWHM (V)	0.089014	0.089018 *Sx < 10^{-9}*	0.089018 *Sx < 10^{-9}*
G = -S = -1 $\theta = 1 = \phi(\theta)$	Ep vs E^0 (V) *	0.025249	0.024280 *Δ = 0.000969* *Sx = 0.000015*	0.0242596 *Δ = 0.0009894* *Sx = 0.0000052*
	B	-1	- 1.00146 *Δ = 0.00146* *Sx = 0.00088*	- 0.99993 *Δ = 0.00007* *Sx = 0.00031*
	Γ (10^{-10} mol.cm^{-2})	5	4.9896 *Δ = 0.0104* *Sx = 0.0012*	4.99996 *Δ = 0.00004* *Sx = 0.00042*
	ip (µA)	6.36897	6.3526 *Δ = 0.0164* *Sx = 0.0023*	6.36910 *Δ = 0.00013* *Sx = 0.00084*
	FWHM (V)	0.143314	0.145966 *Δ = 0.002652* *Sx = 0.000052*	0.143310 *Δ = 0.000004* *Sx = 0.000017*

** From a statistical standpoint, the true value of each parameter is based on a 95% confidence interval, according to:* $\text{estimated} \pm Sx \cdot t_{student}(5\%; \nu)$ with $\nu = \text{number of points} - 1$

Table 3: Results of the fitting processes ($\frac{k}{v} \to \infty$, n = 1, k_0 = 1000 s^{-1}, v = 0.1 $V.s^{-1}$, E^0= 0 V, T = 293 K, A = 0.2 cm^2 and Γ_{max} = 5 10^{-10} $mol.cm^{-2}$) in the case of G = -S = +0.85, $\theta = 0.75 = \phi(\theta)$ and σ_{noise} = 0.5 µA

Condition	Parameters	Simulated	GLI Function	rec-GLI Function
G = -S = +0.85 $\theta = 0.75 = \phi(\theta)$ σ_{noise} = 0.5 µA	Ep vs E^0 (V) *	-0.01610	-0.01585 *Δ = 0.00025* *Sx = 0.00014*	-0.01590 *Δ = 0.00020* *Sx = 0.00014*
	B	0.6375	0.582 *Δ = 0.056* *Sx = 0.010*	0.6086 *Δ = 0.0289* *Sx = 0.0094*
	Γ (10^{-10} $mol.cm^{-2}$)	3.75	3.849 *Δ = 0.099* *Sx = 0.022*	3.815 *Δ = 0.065* *Sx = 0.021*
	Ip (µA)	10.518	10.376 *Δ = 0.142* *Sx = 0.097*	10.480 *Δ = 0.038* *Sx = 0.091*
	FWHM (V)	0.05549	0.05926 *Δ = 0.0377* *Sx = 0.00050*	0.05698 *Δ = 0.00149* *Sx = 0.00049*

** From a statistical standpoint, the true value of each parameter is based on a 95% confidence interval, according to:* $\text{estimated} \pm Sx \cdot t_{student}(5\%; \nu)$ with $\nu = \text{number of points} - 1$

Recursive Function for Fitting Electroactive Monolayer Cyclic Voltammograms and Extracting Key Parameters

Olivier Alévêque and Eric Levillain

Univ Angers, CNRS, MOLTECH-ANJOU, SFR MATRIX, F-49000 Angers, France

Corresponding authors:

olivier.aleveque@univ-angers.fr (Olivier ALEVEQUE)

Tel.: (+33)241735090; Fax: (+33)241735405

eric.levillain@univ-angers.fr (Eric LEVILLAIN)

Tel.: (+33)241735095; Fax: (+33)241735405

FIGURES

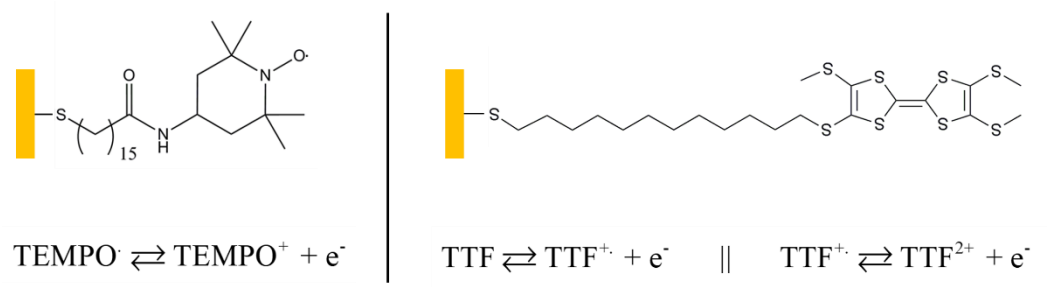

Scheme 1:

TEMPO-based SAM (C15-TEMPO) and TTF-based SAM (C12-TTF) on a gold substrate, along with their corresponding electrochemical processes.

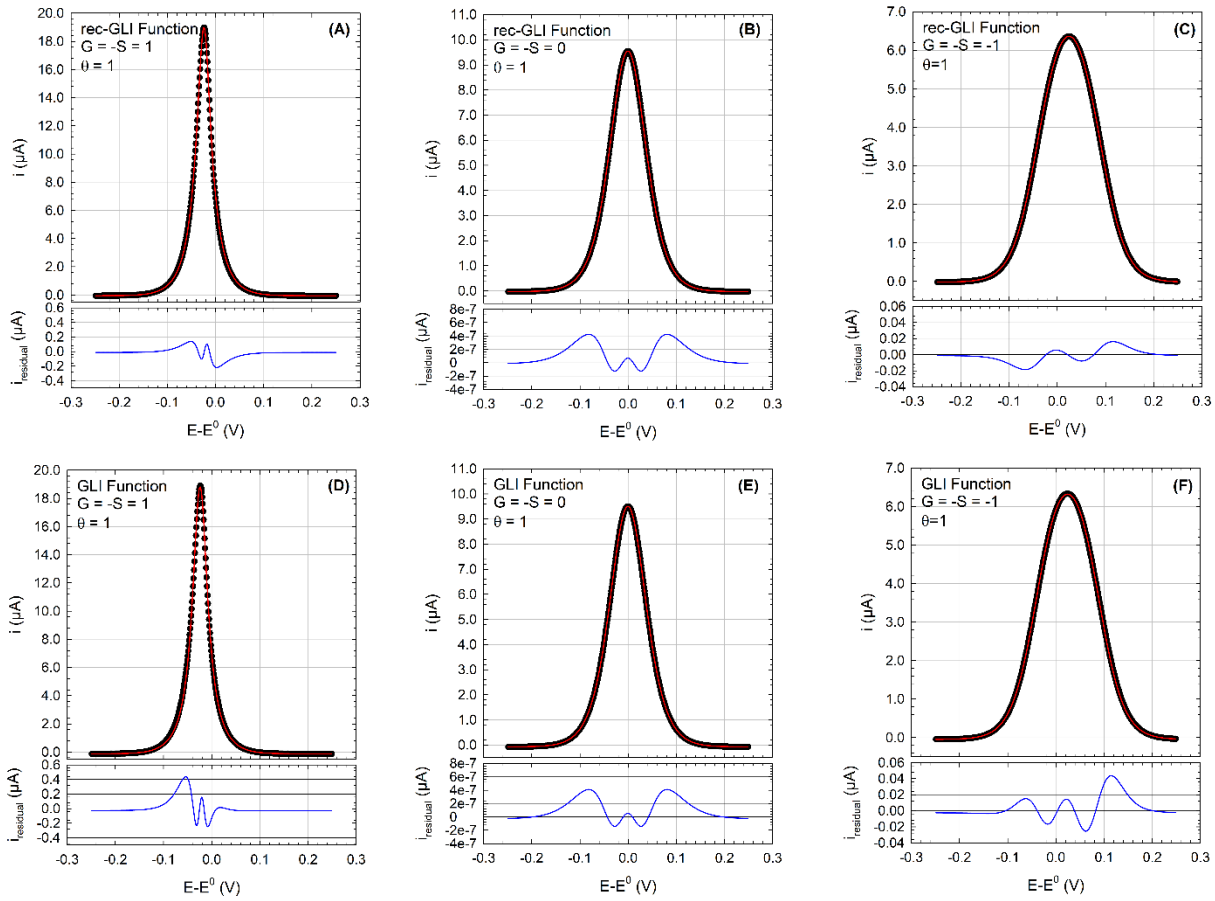

Figure 1:

Evaluation of peak fitting (A, B, C) of the rec-GLI function on simulated cyclic voltammograms (CVs) generated from the GLI model under conditions of a fully reversible reaction ($\frac{k^{0'}}{v} \to \infty$, n = 1, $k^{0'}$ = 1000 s^{-1}, v = 0.1 $V.s^{-1}$, $E^{0'}$ = 0 V, T = 293 K, A = 0.2 cm^2 and Γ_{max} = 5 10^{-10} $mol.cm^{-2}$) in the case of G = -S = {+1 ; 0 ; -1} and $\theta = 1 = \phi(\theta)$, and comparison to GLI function peak fitting (D, E, F). (●) Gaussian noisy simulated points and (—) fitted curves using rec-GLI function or GLI function. The bottom panels/graphs correspond to residual currents, which in our case, are calculated as the difference between the simulated current and the fitted currents.

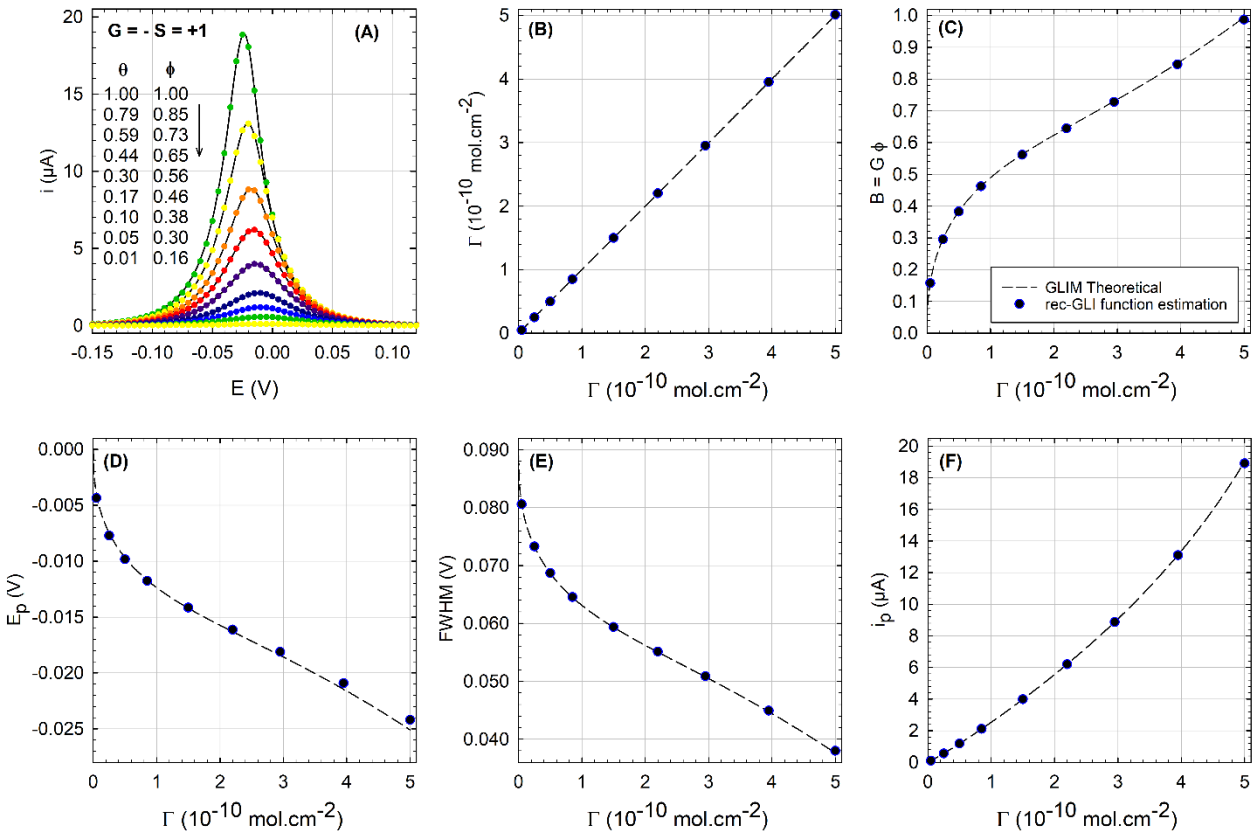

Figure 2: Evaluation of peak fitting of the rec-GLI function on simulated CVs generated from the GLI model under conditions of a fully reversible reaction ($\frac{k^{0'}}{v} \to \infty$, n = 1, $k^{0'}$ = 1000 s^{-1}, v = 0.1 $V.s^{-1}$, $E^{0'}$ = 0 V, T = 293 K, A = 0.2 cm^2 and Γ_{max} = 5 10^{-10} $mol.cm^{-2}$) in the case of G = -S = +1. **(A)** (lines) simulated CVs with different values of surface coverage (θ) and phase segregation (ϕ), and (dotted lines) fitted curves using rec-GLI function. Comparison of (---) theoretical, (●) fitted estimated parameters: **(B)** surface coverage, **(C)** B = G ϕ parameter, **(D)** peak potential, **(E)** full width at half maximum and **(F)** peak intensity

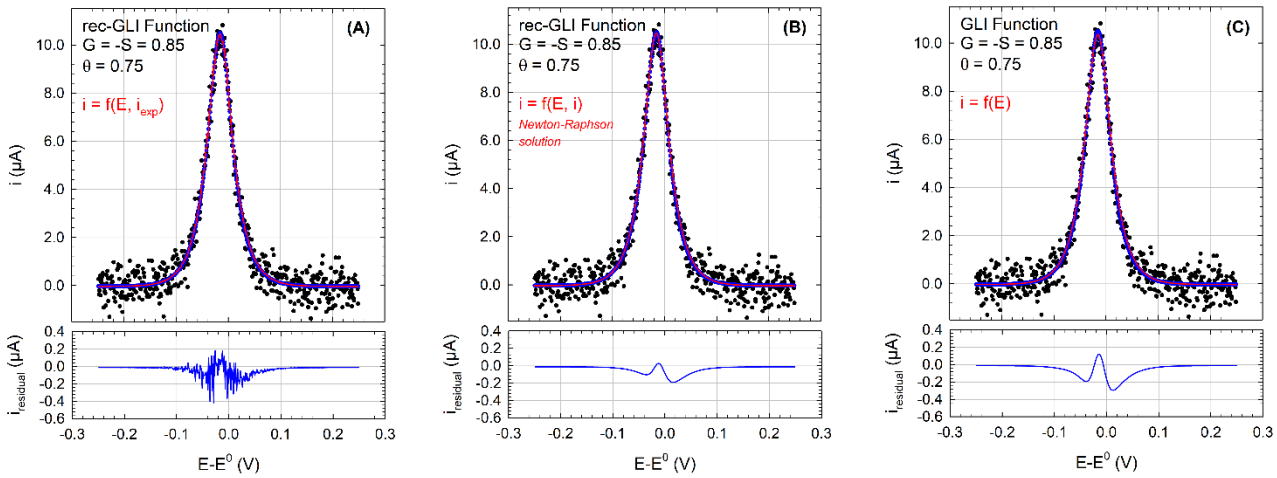

Figure 3: Evaluation of peak fitting (A and B) of the rec-GLI function on Gaussian noisy simulated CVs generated from the GLI model under conditions of a fully reversible reaction (σ_{noise} = 0.5 μA, $\frac{k^{0'}}{v} \rightarrow \infty$, n = 1, $k^{0'}$ = 1000 s^{-1}, v = 0.1 $V.s^{-1}$, $E^{0'}$ = 0 V, T = 293 K, A = 0.2 cm^2 and Γ_{max} = 5 10^{-10} $mol.cm^{-2}$) in the case of G = -S = +0.85, $\theta = 0.75 = \phi(\theta)$, and comparison to GLI function peak fitting (C). (●) Gaussian noisy simulated points, (●) noiseless simulated points and (—) fitted curves using rec-GLI function, replotted with rec-GLI function (A) or Newton-Raphson algorithm solution (B) and fitted curves using GLI function (C). The bottom panels/graphs correspond to residual currents, which in our case, are calculated as the difference between the noiseless simulated currents and the recalculated currents.

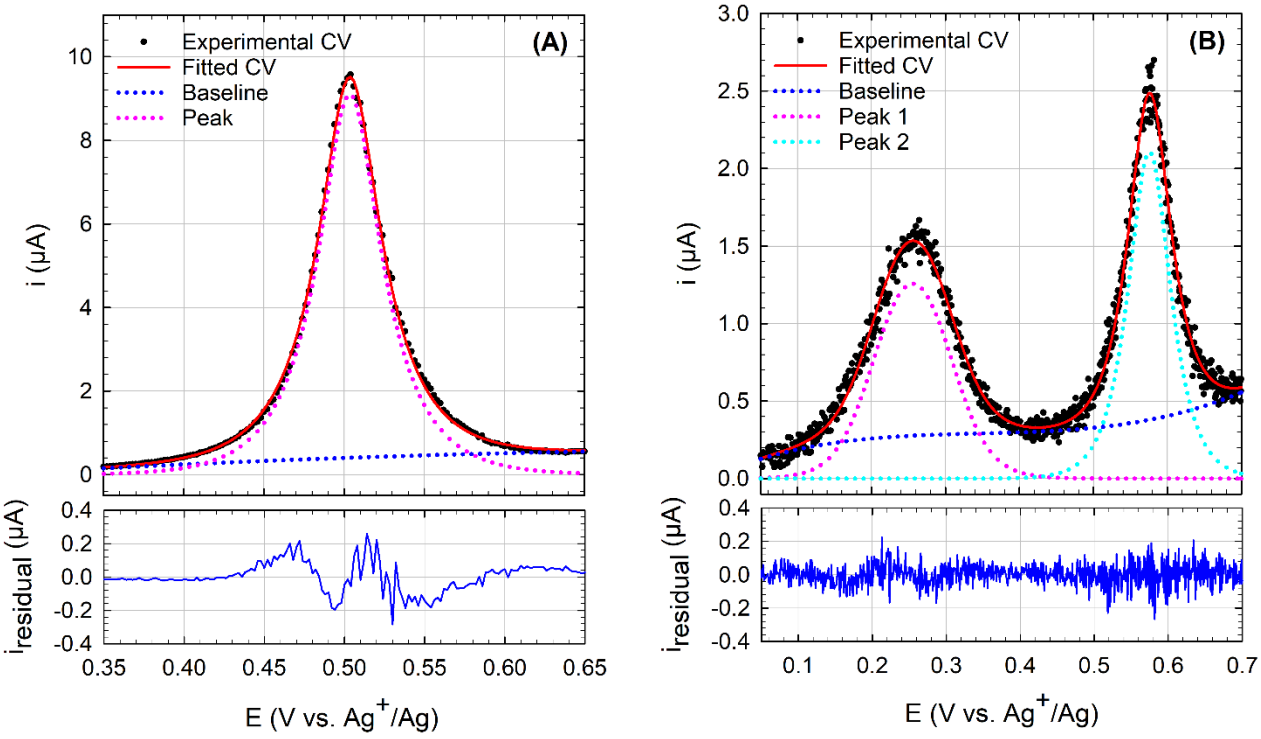

Figure 4: Evaluation of peak fitting of the rec-GLI function on experimental CVs of TEMPO and TTF SAMs in 0.1 M Bu_4NPF_6/CH_2Cl_2, at v = 0.1 $V.s^{-1}$, T = 293 K and A = 0.2 cm^2.

(A) Electrochemical parameters deduced from one peak fitting using rec-GLI function on TEMPO SAM: Γ = 2.91 10^{-10} $mol.cm^{-2}$, B = 0.805, E_{p1} = 0.504 V, FWHM = 0.047 V, i_p = 9.13 µA (*for comparison with GLI function: Γ = 2.89 10^{-10} $mol.cm^{-2}$, B = 0.805, E_{p1} = 0.504 V, FWHM = 0.047 V, i_p = 9.06 µA*)

(B) Electrochemical parameters deduced from two peaks fitting using rec-GLI function on TTF SAM: Γ = 0.88 10^{-10} $mol.cm^{-2}$, B_1 = -0.633, E_{p1} = 0.256 V, $FWHM_1$ = 0.123 V, i_{p1} = 1.25 10^{-6} A, B_2 = 0.426, E_{p2} = 0.576 V, $FWHM_2$ = 0.066 V, i_{p2} = 2.10 10^{-6} A. (*for comparison with GLI function: Γ = 0.88 10^{-10} $mol.cm^{-2}$, B_1 = -0.634, E_{p1} = 0.256 V, $FWHM_1$ = 0.123 V, i_{p1} = 1.25 µA, B_2 = 0.426, E_{p2} = 0.575 V, $FWHM_2$ = 0.066 V, i_{p2} = 2.09 µA*)